

StereoVLA: Enhancing Vision-Language-Action Models with Stereo Vision

Shengliang Deng^{1,3*} Mi Yan^{1,2*} Yixin Zheng^{1,4,5*} Jiayi Su^{1,6} Wenhao Zhang^{1,2}
 Xiaoguang Zhao⁴ Heming Cui³ Zhizheng Zhang^{1,5†} He Wang^{1,2,5†}

Abstract—Stereo cameras closely mimic human binocular vision, providing rich spatial cues critical for precise robotic manipulation. Despite their advantage, the adoption of stereo vision in vision-language-action models (VLAs) remains underexplored. In this work, we present StereoVLA, a VLA model that leverages rich geometric cues from stereo vision. We propose a novel Geometric-Semantic Feature Extraction module that utilizes vision foundation models to extract and fuse two key features: 1) geometric features from subtle stereo-view differences for spatial perception; 2) semantic-rich features from the monocular view for instruction following. Additionally, we propose an auxiliary Interaction-Region Depth Estimation task to further enhance spatial perception and accelerate model convergence. Extensive experiments show that our approach outperforms baselines by a large margin in diverse tasks under the stereo setting, and demonstrates strong robustness to camera pose variations. Our project page is at <https://shengliangd.github.io/StereoVLA-Webpage>.

I. INTRODUCTION

Vision-Language-Action (VLA) models offer an end-to-end framework that maps visual inputs and language instructions to actions, enabling robots to learn diverse skills from demonstrations. Leveraging pretrained Vision-Language Models (VLMs) [1], [2], they exhibit strong generalization and semantic understanding capabilities. Nonetheless, to align with the pretraining paradigm of VLMs, pioneering VLA models (e.g., OpenVLA [3]) rely on single-view RGB image as visual input, limiting accurate geometry perception essential for manipulation. Consequently, providing VLA models with rich geometric cues while preserving their generalization capabilities remains a key challenge.

Previous works mainly explored three types of supplementary sensors: wrist-mounted cameras [4]–[6], depth sensors [7], [8], and extra third-person cameras [9]. However, as shown in Figure 1, wrist cameras provide limited views that are easily occluded, and the wrist-mounted hardware increases collision risk with the environment. Depth sensors yield noisy measurements for transparent or specular objects. Extra third-person cameras offer complementary information, but it complicates hardware design for mobile robots and humanoids, and the increased view diversity hinders generalization to camera poses [10]. These limitations motivate us to revisit human-inspired perception: stereo vision offers robust spatial cues via binocular disparity and captures global scene without additional hardware.

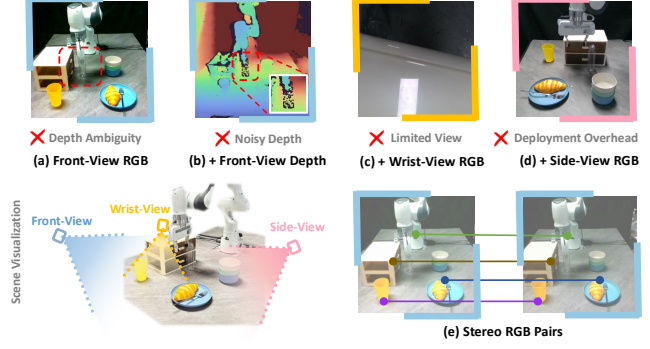


Fig. 1: Common camera setups for robotic manipulation. (a) Single-view RGB suffers from depth ambiguity; (b) depth sensors yield noisy estimates for transparent objects; (c) wrist-view RGB captures a limited view and the additional hardware increases collision risk; (d) multi-camera settings incur additional deployment overhead. (e) Stereo RGB pairs provide robust spatial cues for comprehensive scene understanding, mitigate view limit and collision risk, while enabling a simpler setup with a single stereo camera.

Despite these advantages, stereo vision is rarely exploited in VLAs. Existing works have introduced minimal stereo data [11] into large-scale pretraining mixtures, without a systematic evaluation of the benefits brought by stereo cues. In contrast, stereo-based perception has been a long-standing topic in computer vision, where numerous foundation models [12] for depth estimation have established mature architectural and pretraining paradigms. However, the integration of these strong stereo representations into robot learning frameworks, especially VLA models, remains underexplored.

In this work, we present StereoVLA, a vision-language-action model that exploits rich geometric cues from stereo vision. Due to the subtle differences between stereo views, directly providing stereo inputs to existing multi-camera VLAs (such as $\pi_{0.5}$ and GraspVLA) yields suboptimal performance. To overcome this, we introduce a novel **Geometric-Semantic Feature Extraction** module. It extracts carefully selected dense geometric features from FoundationStereo [12], a state-of-the-art model pretrained on millions of stereo pairs. To complement the geometric-centric features of FoundationStereo with rich semantics for language understanding, we further integrate semantically rich visual tokens from PrismaticVLM [13]. By spatially aligning and fusing these modalities, Geometric-Semantic Feature Extraction

¹Galbot ²Peking University ³ The University of Hong Kong ⁴ Institute of Automation, Chinese Academy of Sciences ⁵ Beijing Academy of Artificial Intelligence ⁶ Xiamen University Malaysia

generates hybrid tokens that effectively combine geometry precision with semantics richness.

To improve manipulation precision through better geometric understanding, we introduce an auxiliary co-training task,

Interaction-Region Depth Estimation, which predicts the metric depth of given points. Rather than sampling points uniformly that often selects uninformative backgrounds, we restrict sampling to the interaction region around the gripper-object pair. This encourages the model to focus on critical spatial details and improves training efficiency.

Evaluation shows that our approach significantly outperforms baselines under stereo configuration, achieving a 33% higher success rate on general tasks and notable improvements in precision-demanding scenarios, and demonstrates strong robustness to camera pose variations. Ablation studies validate the effectiveness of the proposed components.

In summary, our contributions are as follows: a) we introduce StereoVLA, a VLA model that exploits rich geometric cues from stereo vision, b) we introduce Geometric-Semantic Feature Extraction to produce visual tokens that carry dense semantic and geometric features from stereo inputs, c) we propose Interaction-Region Depth Estimation as a co-training task to help the model capture fine-grained spatial details, d) we show that our approach outperforms existing VLAs by a large margin in diverse tasks under stereo settings, and is robust to camera pose variations.

II. RELATED WORK

A. Vision-Language-Action Models

Driven by the rapid progress of vision-language models [1], [2], [13]–[17] and the availability of broad robot datasets [11], [18]–[21], the vision-language-action paradigm [3], [4], [9], [22]–[29] has emerged as a natural way to equip robots with generalizable multimodal reasoning and control. Early systems [3], [22] generated actions by discretizing continuous control for autoregressive prediction, while later approaches [4], [9], [23]–[28] adopted diffusion- or flow-based policies to directly sample smooth trajectories.

Camera configurations in VLAs have likewise expanded to capture richer spatial information. Early models [3], [22] relied on a single overhead RGB view, followed by wrist-mounted monocular cameras [23]–[26], [28], side-facing cameras [9], [27], and the four-corner layout with front and rear perspectives introduced by $\pi_{0.5}$ [4]. Despite this progression from monocular to multi-view sensing, no prior work has exploited stereo cameras, the very mechanism that enables human-level spatial perception.

B. Robot Learning with Geometry Cues

A growing body of work seeks to overcome the inherent limitations of monocular RGB perception by incorporating geometry cues such as depth, point clouds, or reconstructed 3D structure. These geometry-aware inputs provide explicit spatial information that improves robustness, perception, and generalization in visuomotor policy learning. For example, DP3 [30] show that leveraging point-cloud observations enhances robustness to lighting and object variations, while

iDP3 [31] extends it by adopting a robot-centered egocentric frame, reducing sensitivity to environmental variations and enabling robust 3D perception from both egocentric and third-person viewpoints.

Building on this insight, recent VLA research has begun to fuse geometry cues with language and action to address the spatial reasoning limitations of purely 2D models. Several approaches [8], [32]–[37] explore joint reasoning over geometry, semantics, and control. For instance, 3D-VLA [8] unifies 3D perception, reasoning, and control within a large-scale 3D language model trained on diverse embodied-robot datasets. PointVLA [33] augments VLA systems with depth cues from RGB-D sensors or monocular depth estimation to improve spatial understanding and geometry-aware manipulation, while BridgeVLA [34] projects 3D observations into multi-view 2D feature maps and predicts actions through 2D heatmaps, yielding strong sample efficiency and real-robot transfer. However, most existing methods have yet to thoroughly explore how to effectively fuse explicit geometry cues with the rich 2D representations of pretrained vision foundation models.

C. Stereo Perception and Policies for Robot Learning

Deep stereo matching has evolved from cost-volume aggregation with 3D CNNs [38]–[43], which are accurate but memory-intensive, to RAFT-style [44] iterative refinement [45]–[49] that avoids explicit 4D volumes while preserving precision. More recently, FoundationStereo [12] leverages large-scale vision pretraining to achieve strong generalization.

In parallel, stereo-driven policies exploit stereo images for robotic manipulation. Stereo visual-servoing [50] maps 2D stereo features to joint commands for depth-aware grasping without explicit 3D reconstruction. DextrAH-RGB [51] learns stereo-based visuomotor control for grasping through teacher-student distillation, transferring robustly to real robots. SimNet [52] uses large-scale synthetic stereo data to predict disparity, segmentation, 3D bounding boxes, and keypoints, supporting reliable grasping of unseen objects.

While prior stereo-policy frameworks are typically based on small-scale architectures, our work scales this paradigm to large vision-language-action models, where the increased model capacity and vision-language grounding capability jointly contribute to stronger spatial awareness, cross-task generalization, and multimodal understanding.

III. METHOD

The overall architecture of StereoVLA is illustrated in Figure 2(a). The **Geometric-Semantic Feature Extraction** module leverages state-of-the-art vision foundation models to encode the stereo images into visual tokens that capture both semantic and geometric information. These visual tokens, together with language tokens, are passed to a pre-trained large language model, InternLM-1.8B [53], for vision-language joint processing. Leveraging the intermediate vision-language features (i.e., the key-value cache), a 300M-parameter action expert predicts action chunks via

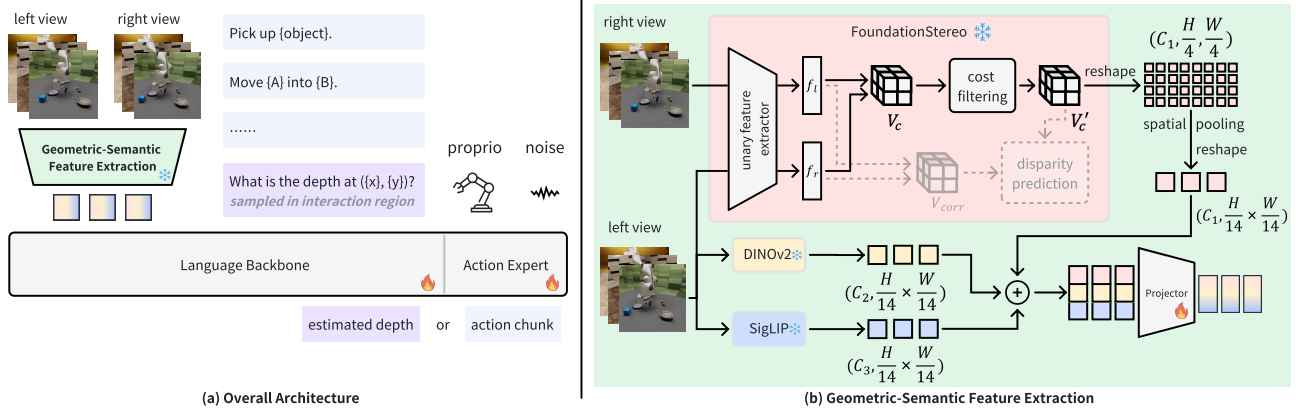


Fig. 2: (a) In StereoVLA, a stereo image pair is encoded by the Geometric-Semantic Feature Extraction module to generate visual tokens with geometric precision and semantic richness. Together with language tokens, they are processed by a large language model backbone (InternLM-1.8B). An action expert predicts delta end-effector poses, while an auxiliary depth estimation task further enhances geometry learning during training. (b) The Geometric-Semantic Feature Extraction module extracts geometric features with FoundationStereo (bypassing disparity prediction components for efficiency) and semantic-rich features with SigLIP and DINOv2, then fuses them into a unified visual representation with an MLP projector.

flow-matching [23], [54] with a delta end-effector pose representation. To further enhance geometry learning, we introduce an auxiliary co-training task, **Interaction-Region Depth Estimation**, which improves fine-grained geometric understanding while preserving training and inference efficiency.

A. Geometric-Semantic Feature Extraction

As shown in Figure 2(b), given a stereo image pair $I_l, I_r \in \mathbb{R}^{H \times W \times 3}$, we carefully extract geometric features from FoundationStereo [12] from both views and semantic-rich features from the monocular left view I_l . These features are then fused into a sequence of visual tokens that jointly encode both geometric and semantic information.

Geometric Feature Extraction. FoundationStereo is tailored for depth estimation with several specialized modules, making feature adaptation to our task non-trivial. We therefore first outline the key components of FoundationStereo and then explain our feature choices.

For stereo image pairs I_l, I_r , FoundationStereo first computes monocular features f_l, f_r for each image with a unary feature extractor. These features are then processed via two parallel paths. In the first path, f_l, f_r are concatenated to form a 4D cost volume $V_c \in \mathbb{R}^{C \times \frac{D}{4} \times \frac{H}{4} \times \frac{W}{4}}$, where H and W denote the image height and width, D is the maximum disparity range considered, and C is the feature dimension. To model long-range correlations, the cost volume undergoes an attention-based hybrid cost filtering module, yielding a filtered cost volume V'_c with the same dimensions. In the second path, the dot product of the left and right unary features f_l, f_r are computed to generate a correlation volume $V_{corr} \in \mathbb{R}^{\frac{W}{4} \times \frac{H}{4} \times \frac{W}{4}}$. Using the filtered cost volume V'_c and correlation volume V_{corr} , FoundationStereo iteratively refines disparity estimates, resulting in a final disparity map.

When selecting features, we consider two criteria: (1) they should be dense feature volumes and capture rich geometric information, and (2) additional computation for depth estimation should be minimized.

Guided by these criteria, we choose the filtered cost volume V'_c as our geometric feature source. Although the iterative refinement in FoundationStereo further improves disparity estimation, it introduces considerable computational overhead. Similarly, the correlation volume V_{corr} consists of matching scores rather than dense features, so we discard the second computation path. From the first path, we choose V'_c over the raw cost volume V_c because it incorporates long-range correlations via the hybrid cost filtering module, providing dense geometric features crucial for manipulation.

Semantic Feature Extraction. As FoundationStereo is pretrained for depth estimation, it lacks the semantic and appearance information for effective vision-language grounding. To overcome this, we extract these features using SigLIP and DINOv2 following PrismaticVLM [13]. SigLIP, trained with a vision-language contrastive objective, effectively captures high-level semantics. DINOv2, trained with self-supervised discriminative objectives that align features across different image crops, excels at capturing visual details [13], [55]. Due to the high redundancy of the semantic and visual appearance information between left and right views, we apply SigLIP and DINOv2 exclusively on the left view for computational efficiency.

Feature Fusion. The spatial resolution of FoundationStereo features differ with those of SigLIP and DINOv2. We therefore spatially pool the FoundationStereo features to match the 14-pixel stride of the other two. The final hybrid representation is obtained by concatenating the feature maps along the channel dimension. We avoid token sequence concatenation, as it increases the number of tokens and computational overhead during both training and inference.

B. Interaction-Region Depth Estimation

To strengthen the model’s ability to capture fine-grained geometric information essential for manipulation, we introduce an auxiliary task, Interaction-Region Depth Estimation. This task is co-trained with action chunk prediction, ensuring no extra computational overhead during inference.

In this task, the large language model is trained to predict the metric depth d of a sampled point (x, y) , utilizing the ground-truth depth from our synthetic dataset. A naive approach is to uniformly sample points across the entire image. However, this often samples from the background (e.g., tables, walls) that provide little task-relevant information.

To overcome this, we restrict sampling to the *interaction region*, i.e., the area encompassing both the gripper and the target object, identified by the object’s 2D bounding box. This focused sampling encourages the model to reason about the object’s geometry and its spatial relationship with the gripper, benefiting manipulation precision and convergence.

C. Dataset Curation

Existing large-scale robotic datasets, such as Open-X [56] and AgiBot-World [19], do not provide stereo image pairs. To overcome this, we follow GraspVLA and use MuJoCo [57] to generate synthetic pick-and-place action sequences, rendering stereo observations with Isaac Sim [58]. In data generation, the baseline and intrinsic matrix of the stereo camera is configured to randomize within a 5% range of those of our real Zed Mini camera. The camera poses are described in Section IV-B. The images are rendered in 256x256 resolution, and resized to 224x224 for pretrained DINOv2 and SigLIP. We generate 5 million synthetic trajectories recorded at 10Hz. Furthermore, following GraspVLA, we incorporate the Internet-scale grounding dataset GRIT [59] and add 2D bounding box prediction as an auxiliary task to enhance the model’s semantic grounding capability.

D. Training Details

Following GraspVLA, we adopt progressive action generation, where the model first predicts the 2D bounding box of the target object and the next keyframe pose of the gripper as intermediate steps to guide action chunk prediction. Since the left and right stereo images contain largely redundant semantic information, we only require the model to predict the bounding box on the left image to reduce computational overhead. The overall training loss is defined as

$$\mathcal{L} = \mathcal{L}_{action} + \mathcal{L}_{depth} + \mathcal{L}_{bbox} + \mathcal{L}_{pose}, \quad (1)$$

where \mathcal{L}_{action} is the flow-matching loss for action chunk prediction, and \mathcal{L}_{depth} , \mathcal{L}_{bbox} , and \mathcal{L}_{pose} are cross-entropy losses for depth estimation, bounding box prediction, and keyframe pose prediction, respectively. We balance samples from the four tasks with a ratio of 5:2:2:1. The model is trained for 160k steps on 32 NVIDIA H800 GPUs with a batch size of 384 and a learning rate of 1.6e-4.

IV. EVALUATION

We conduct comprehensive experiments to answer three key questions: 1) How does StereoVLA compare to existing VLAs on representative manipulation tasks? 2) How does the stereo camera setting compare to other camera settings under comparable training conditions with state-of-the-art VLAs? 3) What is the individual contribution of our proposed design components to the overall performance?

A. Real-world Experiments

1) *Task Suite*: We evaluate the language understanding and manipulation abilities with a set of **General Tasks**, including picking/placing common objects (such as bread and toy dinosaur), stacking cubes and bowls, etc.

To evaluate with tasks requiring higher precision, we design two additional categories of tasks:

Grasping bar-shaped objects. Bar-shaped objects, such as pens and forks, have a significantly larger length compared to their width or thickness. Their short axis demands precisely estimating the spatial relationship between the gripper and the object, while the long axis often leads to visual overlap with the gripper in camera views, and misleads the model to grasp at improper positions. To systematically evaluate the performance, we test with objects oriented at 0°, 45°, and 90° relative to the camera.

Grasping medium and small objects. This category includes medium-sized (3 ~ 5 cm) and small (1 ~ 2 cm) objects, which require especially high precision in both perception and actions.

2) *Hardware Setup*: The hardware setup is shown in Figure 4. Target objects and distractors are placed in a workspace sizing 0.5m × 0.4m. To systematically evaluate the impact of camera settings, we introduce three levels of pose randomization for both front and side cameras, as shown in the figure. Unless otherwise specified, we employ the small randomization range. Results for all randomization ranges are reported in Section IV-B.

3) *Baselines*: Since no existing VLAs target the stereo camera setup, we train/finetune state-of-the-art open-source VLAs with our full synthetic stereo dataset for a fair comparison. SpatialVLA [32] is designed to explicitly leverage depth, but its original design relies on estimated depth from a single RGB image, which could result in inaccurate estimations due to lack of direct depth cues. Therefore, we additionally introduce a variant denoted as SpatialVLA-D (“D” stands for depth), which utilizes high-quality depth estimated from the stereo input with FoundationStereo. $\pi_{0.5}$ [4] is a generalist for its strong adaptability. GraspVLA [9] features large-scale synthetic dataset pretraining. We adapt $\pi_{0.5}$ and GraspVLA [9] by providing the left and right views as their multi-view inputs, denoted as $\pi_{0.5}$ -S and GraspVLA-S (“S” for stereo). $\pi_{0.5}$ -S, SpatialVLA, and SpatialVLA-D are finetuned using their recommended hyper-parameters. GraspVLA-S is trained from the VLM initialization, as its released checkpoint is for front + side view settings.

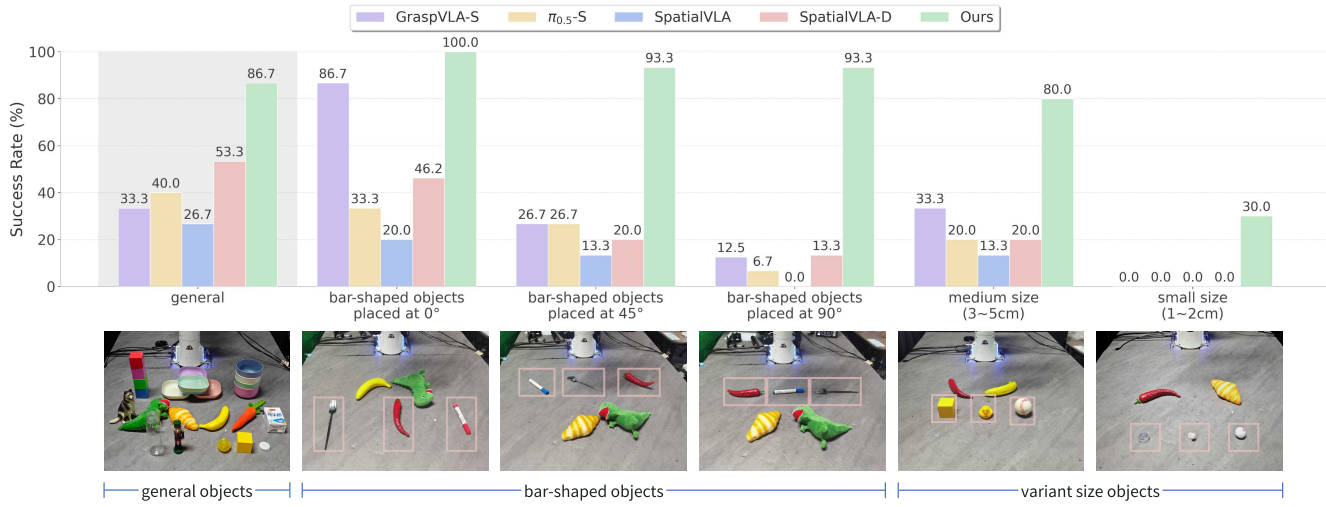


Fig. 3: **Real-world evaluation tasks and results.** We evaluate StereoVLA on a comprehensive suite of tasks requiring fine-grained perception and manipulation, including grasping bar-shaped objects at various orientations, grasping objects of medium and small sizes, and general-purpose pick-and-place scenarios. Objects enclosed by colored boxes denote the target objects used for evaluation, while other items in the scene serve as distractors. StereoVLA consistently achieves the highest success rate across all task types, highlighting the effectiveness of our method.

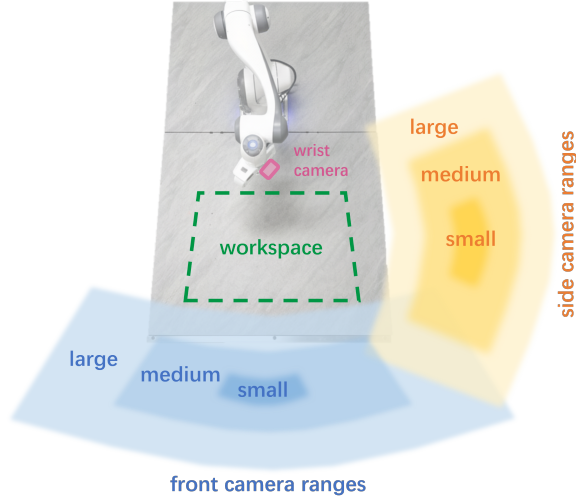


Fig. 4: **Layout of the robot arm, workspace, and cameras.** To study method robustness to viewpoint changes, we define three randomization ranges for the front and side cameras.

4) Metrics: Task success rates are reported for each test set, with 15 trials per set, yielding a total of $15 \times 6 \times 5 = 450$ trials. To rigorously assess fine-grained spatial perception and manipulation, we incorporate three additional criteria. First, to prevent models from succeeding through repeated attempts, each trial allows only a single execution - one gripper-close before grasping and one gripper-open after grasping. Second, we disable the “gripper sticking” heuristic used in OpenVLA, SpatialVLA, and $\pi_{0.5}$, since it artificially delays gripper actions and can conceal inaccurate decisions. Third, a trial is deemed successful only when the task

is fully completed, with no partial credit assigned. While these stricter criteria produce lower success rates than those reported in prior work, they provide a more accurate measure of model capability.

5) Results: Figure 3 shows the success rates across the evaluation tasks. StereoVLA achieves the strongest and most consistent performance. For bar-shaped objects at 0°, 45°, and 90° orientations, StereoVLA achieved near-perfect or perfect results. In contrast, other baselines, including GraspVLA-S, $\pi_{0.5}$ -S, and SpatialVLA-(D), performed noticeably worse. Besides, success rates decreased for all models as the object orientation increased. This is because the grasping is more sensitive to depth estimation errors when bar-shaped objects are placed at angles closer to 90°.

On the most challenging task of grasping small objects, StereoVLA achieved a 30.0% success rate even if only a single trial is allowed, while all other baselines completely failed. Further improving the performance would require increasing the image resolution, as small objects span only a few pixels in the current 224×224 resolution, limiting the fidelity of semantic grounding and localization. While employing higher-resolution vision backbones could mitigate this, it entails major increases in computational cost; optimizing this trade-off is an important direction for future work.

6) Qualitative Analysis: $\pi_{0.5}$ and the original SpatialVLA model often approached correct target objects, but consistently closed the gripper too early, likely due to the lack of precise spatial perception. SpatialVLA-D, despite being given superior stereo-derived depth, still struggled, possibly due to the loss of fine geometric detail as it down-samples the depth during spatial encoding.

GraspVLA-S, which encodes left and right images independently, performed well when grasping bar-shaped objects

feature	w/o sem.	w/ sem.
V_{corr}	27.0%	54.0%
V_c	40.0%	69.0%
V'_c	51.0%	77.0%

TABLE I: **Comparison of feature selections.** The adoption of the filtered cost volume V'_c and the semantic feature results in the highest success rate.

placed at 0° , but was much worse on other tasks. We hypothesize that GraspVLA’s additional supervision of grasping poses enhanced the model’s spatial perception capability, yet unable to consistently capture the fine-grained spatial relationship from the subtle differences between stereo views.

Overall, these results suggest that the superior performance of StereoVLA stems from methodological innovations rather than from data scale or quality, emphasizing the critical role of model architectures and training strategies in the stereo setting.

B. Comparison of Camera Settings

While our approach shows strong performance under stereo settings, it is important to compare how different camera settings impact VLA task performance. Previous work offers limited comparisons across camera setups mainly due to scarce data for each setup. We compare four common configurations [3], [4], [9], [32], [56]: single-view (SpatialVLA-D), stereo (StereoVLA), front + wrist (retrained GraspVLA and finetuned $\pi_{0.5}$), and front + side (GraspVLA).

To study the robustness to camera pose variations, we generate equal-sized datasets with three camera pose randomization ranges (Figure 4) and train/finetune each model accordingly. The camera pose ranges are designed as spherical shells around the workspace, which can be approximated as cuboids for ease of description. For the front view, the small range corresponds to approximately a $15 \times 10 \times 15$ cm cuboid, while the large configuration extends to $150 \times 50 \times 60$ cm. Similarly, for the side view, the small range maintains dimensions of $15 \times 10 \times 15$ cm, and the large configuration spans $100 \times 50 \times 60$ cm.

Average task success rates are reported in Table II. While the front + side configuration with GraspVLA yields the best results with small randomization, it suffers a significant drop in larger randomization due to the difficulty of extracting coherent spatial cues from unaligned views. In contrast, StereoVLA achieves comparable performance under small camera pose randomization, and ranks the highest in both medium and large ranges, demonstrating strong robustness to camera pose variations.

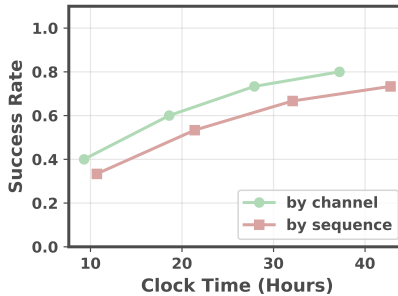


Fig. 5: **Comparison of feature fusion methods.** Sequence concatenation results in a slightly lower success rate and requires a longer training time.

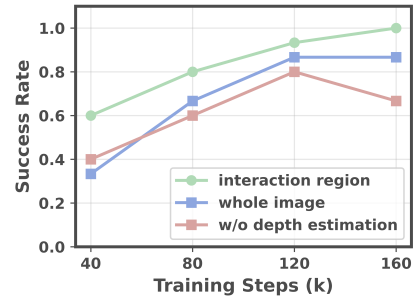


Fig. 6: **Comparison of depth estimation methods.** Depth estimation within the interaction region yields the highest success rate.

TABLE II: **Comparison of camera settings.** StereoVLA demonstrates superior robustness to camera pose variations with competitive performance. Best results are **bolded**, second-best results are underlined.

camera settings	model	small	medium	large
single view	SpatialVLA-D [32]	24.6%	13.7%	6.8%
front + wrist	$\pi_{0.5}$ [4]	64.3%	56.5%	51.6%
front + wrist	GraspVLA [9]	71.3%	<u>63.4%</u>	<u>54.8%</u>
front + side	GraspVLA [9]	82.5%	55.7%	24.1%
stereo	StereoVLA	<u>79.3%</u>	71.9%	61.3%

Front + wrist configurations (GraspVLA, $\pi_{0.5}$) perform worse than front + side under small randomization but degrade less as pose variation increases. The wrist camera offers close views of gripper-object interactions but lacks reliable depth information, leading to more early grasps. The single-view setup consistently underperforms, often closing the gripper at incorrect positions, highlighting the inherent limitations of monocular vision in spatially varied tasks.

In summary, these results suggest that the stereo configuration offers the best balance of task performance, robustness to camera pose variation, and deployment simplicity.

C. Design Choices of Geometric-Semantic Feature Extraction

We conduct ablation experiments on the Geometric-Semantic Feature Extraction module to evaluate the effectiveness of our feature selection and fusion strategies.

For the selection of FoundationStereo features, we evaluate models in simulation after 100k training steps, averaging the performance of the three most recent checkpoints at 10k-step intervals. As shown in Table I, success rates progressively improve when using V_{corr} , V_c , and V'_c , respectively. This supports our hypothesis that V_{corr} retains little geometric information, whereas the unfiltered cost volume V_c lacks the long-range spatial relationships present in the filtered version V'_c . The superior performance of V'_c validates our choice of this representation as the stereo feature.

In addition, the results show that incorporating the semantic feature consistently yields higher success rates than

using the stereo feature alone. Manual inspection of the rollouts revealed that models without the semantic feature more frequently grasped incorrect objects, indicating that semantic features is essential for vision-language grounding. This justifies the necessity of fusing both features.

As is shown in Figure 5, for feature fusion strategies, concatenating features by sequence yields slightly lower success rates and increases computational overhead due to the doubled number of visual tokens. Channel-wise concatenation provides both efficiency and performance advantages.

In addition to FoundationStereo [12], other foundation models, such as VGGT [60], can be alternatives for stereo feature extraction. We compare the depth estimation precision of VGGT and FoundationStereo on our dataset to assess their performance in manipulation scenarios. VGGT obtains an AbsRel [61] error of 0.4121, whereas FoundationStereo achieves a substantially lower error of 0.0275. These results indicate that FoundationStereo provides more reliable depth information, likely due to its specialization in stereo inputs. In contrast, VGGT may excel in broader multi-view settings without stereo assumptions.

D. Effectiveness of Interaction-Region Depth Estimation

We further study the effectiveness of Interaction-Region Depth Estimation by comparing with two alternatives: predicting depth of points uniformly sampled in the whole image, and no prediction of depth. As shown in Figure 6, Interaction-Region Depth Estimation facilitates model learning and achieves the highest performance. In contrast, predicting depth over the entire image negatively impacts training in the early stages, potentially due to the additional burden of learning irrelevant background depths that do not contribute to manipulation success. Nevertheless, both depth estimation strategies stabilize training in later stages. This suggests that explicitly supervising the model to perceive critical spatial details is beneficial.

V. LIMITATION AND FUTURE WORK

Despite promising results, our work has several limitations. First, the image resolution of 224×224 yields limited performance on small objects. Adopting a higher resolution while balancing the computational cost is an important future direction. Second, the model does not yet capture long-horizon temporal dependencies, restricting more complex manipulation task execution. Third, the evaluation was performed on a single embodiment (the Franka arm). However, our method itself is not specific to any particular robot and can be applied to a wide range of embodiments.

VI. CONCLUSION

We introduced StereoVLA, a vision-language-action model that exploits rich geometric cues from stereo vision to achieve robust and precise manipulation. Experiments demonstrate that our approach outperforms prior methods by a large margin in the stereo setting, and is robust to camera pose variations. Furthermore, our comparison of camera setups provides practical guidance for balancing task performance and deployment overhead in future studies.

REFERENCES

- [1] L. Beyer, A. Steiner, A. S. Pinto, A. Kolesnikov, X. Wang, D. Salz, M. Neumann, I. Alabdulmohsin, M. Tschanen, E. Bugliarello *et al.*, “Paligemma: A versatile 3b vlm for transfer,” *arXiv preprint arXiv:2407.07726*, 2024.
- [2] S. Bai, K. Chen, X. Liu, J. Wang, W. Ge, S. Song, K. Dang, P. Wang, S. Wang, J. Tang *et al.*, “Qwen2. 5-vl technical report,” *arXiv preprint arXiv:2502.13923*, 2025.
- [3] M. J. Kim, K. Pertsch, S. Karamcheti, T. Xiao, A. Balakrishna, S. Nair, R. Rafailov, E. Foster, G. Lam, P. Sanketi *et al.*, “Openvla: An open-source vision-language-action model,” *arXiv preprint arXiv:2406.09246*, 2024.
- [4] K. Black, N. Brown, J. Darpinian, K. Dhabalia, D. Driess, A. Esmail, M. Equi, C. Finn, N. Fusai, M. Y. Galliker *et al.*, “π0. 5: a vision-language-action model with open-world generalization,” *arXiv preprint arXiv:2504.16054*, 2025.
- [5] J. Bjorck, F. Castañeda, N. Cherniadev, X. Da, R. Ding, L. Fan, Y. Fang, D. Fox, F. Hu, S. Huang *et al.*, “Gr00t n1: An open foundation model for generalist humanoid robots,” *arXiv preprint arXiv:2503.14734*, 2025.
- [6] S. Liu, L. Wu, B. Li, H. Tan, H. Chen, Z. Wang, K. Xu, H. Su, and J. Zhu, “Rdt-1b: a diffusion foundation model for bimanual manipulation,” *arXiv preprint arXiv:2410.07864*, 2024.
- [7] A. Goyal, J. Xu, Y. Guo, V. Blukis, Y.-W. Chao, and D. Fox, “Rvt: Robotic view transformer for 3d object manipulation,” in *Conference on Robot Learning*. PMLR, 2023, pp. 694–710.
- [8] H. Zhen, X. Qiu, P. Chen, J. Yang, X. Yan, Y. Du, Y. Hong, and C. Gan, “3d-vla: A 3d vision-language-action generative world model,” *arXiv preprint arXiv:2403.09631*, 2024.
- [9] S. Deng, M. Yan, S. Wei, H. Ma, Y. Yang, J. Chen, Z. Zhang, T. Yang, X. Zhang, H. Cui *et al.*, “Graspvla: a grasping foundation model pre-trained on billion-scale synthetic action data,” *arXiv preprint arXiv:2505.03233*, 2025.
- [10] A. Xie, L. Lee, T. Xiao, and C. Finn, “Decomposing the generalization gap in imitation learning for visual robotic manipulation,” 2023. [Online]. Available: <https://arxiv.org/abs/2307.03659>
- [11] A. Khazatsky, K. Pertsch, S. Nair, A. Balakrishna, S. Dasari, S. Karamcheti, S. Nasiriany, M. K. Srirama, L. Y. Chen, K. Ellis *et al.*, “Droid: A large-scale in-the-wild robot manipulation dataset,” *arXiv preprint arXiv:2403.12945*, 2024.
- [12] B. Wen, M. Trepte, J. Aribido, J. Kautz, O. Gallo, and S. Birchfield, “Foundationstereo: Zero-shot stereo matching,” in *Proceedings of the Computer Vision and Pattern Recognition Conference*, 2025, pp. 5249–5260.
- [13] S. Karamcheti, S. Nair, A. Balakrishna, P. Liang, T. Kollar, and D. Sadigh, “Prismatic vlms: Investigating the design space of visually-conditioned language models,” in *Forty-first International Conference on Machine Learning*, 2024.
- [14] D. Driess, F. Xia, M. S. Sajjadi, C. Lynch, A. Chowdhery, A. Wahid, J. Tompson, Q. Vuong, T. Yu, W. Huang *et al.*, “Palm-e: An embodied multimodal language model,” 2023.
- [15] Y. Li, F. Wei, C. Zhang, and H. Zhang, “Eagle-2: Faster inference of language models with dynamic draft trees,” *arXiv preprint arXiv:2406.16858*, 2024.
- [16] P. Wang, S. Bai, S. Tan, S. Wang, Z. Fan, J. Bai, K. Chen, X. Liu, J. Wang, W. Ge *et al.*, “Qwen2-vl: Enhancing vision-language model’s perception of the world at any resolution,” *arXiv preprint arXiv:2409.12191*, 2024.
- [17] B. Xiao, H. Wu, W. Xu, X. Dai, H. Hu, Y. Lu, M. Zeng, C. Liu, and L. Yuan, “Florence-2: Advancing a unified representation for a variety of vision tasks,” in *Proceedings of the IEEE/CVF Conference on Computer Vision and Pattern Recognition*, 2024, pp. 4818–4829.
- [18] A. O’Neill, A. Rehman, A. Maddukuri, A. Gupta, A. Padalkar, A. Lee, A. Pooley, A. Gupta, A. Mandlekar, A. Jain *et al.*, “Open x-embodiment: Robotic learning datasets and rt-x models: Open x-embodiment collaboration 0,” in *2024 IEEE International Conference on Robotics and Automation (ICRA)*. IEEE, 2024, pp. 6892–6903.
- [19] Q. Bu, J. Cai, L. Chen, X. Cui, Y. Ding, S. Feng, S. Gao, X. He, X. Hu, X. Huang *et al.*, “Agibot world colosse: A large-scale manipulation platform for scalable and intelligent embodied systems,” *arXiv preprint arXiv:2503.06669*, 2025.
- [20] H.-S. Fang, H. Fang, Z. Tang, J. Liu, C. Wang, J. Wang, H. Zhu, and C. Lu, “Rh20t: A comprehensive robotic dataset for learning diverse skills in one-shot,” *arXiv preprint arXiv:2307.00595*, 2023.

[21] K. Wu, C. Hou, J. Liu, Z. Che, X. Ju, Z. Yang, M. Li, Y. Zhao, Z. Xu, G. Yang *et al.*, “Robomind: Benchmark on multi-embodiment intelligence normative data for robot manipulation,” *arXiv preprint arXiv:2412.13877*, 2024.

[22] B. Zitkovich, T. Yu, S. Xu, P. Xu, T. Xiao, F. Xia, J. Wu, P. Wohlhart, S. Welker, A. Wahid *et al.*, “Rt-2: Vision-language-action models transfer web knowledge to robotic control,” in *Conference on Robot Learning*. PMLR, 2023, pp. 2165–2183.

[23] K. Black, N. Brown, D. Driess, A. Esmail, M. Equi, C. Finn, N. Fusai, L. Groom, K. Hausman, B. Ichter *et al.*, “pi0: A vision-language-action flow model for general robot control,” *arXiv preprint arXiv:2410.24164*, 2024.

[24] K. Pertsch, K. Stachowicz, B. Ichter, D. Driess, S. Nair, Q. Vuong, O. Mees, C. Finn, and S. Levine, “Fast: Efficient action tokenization for vision-language-action models,” *arXiv preprint arXiv:2501.09747*, 2025.

[25] J. Wen, Y. Zhu, J. Li, Z. Tang, C. Shen, and F. Feng, “Dexvla: Vision-language model with plug-in diffusion expert for general robot control,” *arXiv preprint arXiv:2502.05855*, 2025.

[26] J. Liu, H. Chen, P. An, Z. Liu, R. Zhang, C. Gu, X. Li, Z. Guo, S. Chen, M. Liu *et al.*, “Hybridvla: Collaborative diffusion and autoregression in a unified vision-language-action model,” *arXiv preprint arXiv:2503.10631*, 2025.

[27] Q. Li, Y. Liang, Z. Wang, L. Luo, X. Chen, M. Liao, F. Wei, Y. Deng, S. Xu, Y. Zhang *et al.*, “Cogact: A foundational vision-language-action model for synergizing cognition and action in robotic manipulation,” *arXiv preprint arXiv:2411.19650*, 2024.

[28] I.-M. Contributors, “Internvla-m1: Latent spatial grounding for instruction-following robotic manipulation,” 2025.

[29] J. Wen, Y. Zhu, J. Li, M. Zhu, Z. Tang, K. Wu, Z. Xu, N. Liu, R. Cheng, C. Shen, Y. Peng, F. Feng, and J. Tang, “Tinyvla: Toward fast, data-efficient vision-language-action models for robotic manipulation,” *IEEE Robotics Autom. Lett.*, vol. 10, no. 4, pp. 3988–3995, 2025. [Online]. Available: <https://doi.org/10.1109/LRA.2025.3544909>

[30] Y. Ze, G. Zhang, K. Zhang, C. Hu, M. Wang, and H. Xu, “3d diffusion policy: Generalizable visuomotor policy learning via simple 3d representations,” *arXiv preprint arXiv:2403.03954*, 2024.

[31] Y. Ze, Z. Chen, W. Wang, T. Chen, X. He, Y. Yuan, X. B. Peng, and J. Wu, “Generalizable humanoid manipulation with 3d diffusion policies,” *arXiv preprint arXiv:2410.10803*, 2024.

[32] D. Qu, H. Song, Q. Chen, Y. Yao, X. Ye, Y. Ding, Z. Wang, J. Gu, B. Zhao, D. Wang *et al.*, “Spatialvla: Exploring spatial representations for visual-language-action model,” *arXiv preprint arXiv:2501.15830*, 2025.

[33] C. Li, J. Wen, Y. Peng, Y. Peng, F. Feng, and Y. Zhu, “Pointvla: Injecting the 3d world into vision-language-action models,” *arXiv preprint arXiv:2503.07511*, 2025.

[34] P. Li, Y. Chen, H. Wu, X. Ma, X. Wu, Y. Huang, L. Wang, T. Kong, and T. Tan, “Bridgevla: Input-output alignment for efficient 3d manipulation learning with vision-language models,” *arXiv preprint arXiv:2506.07961*, 2025.

[35] R. Yang, G. Chen, C. Wen, and Y. Gao, “Fp3: A 3d foundation policy for robotic manipulation,” *arXiv preprint arXiv:2503.08950*, 2025.

[36] T. Lin, G. Li, Y. Zhong, Y. Zou, and B. Zhao, “Evo-0: Vision-language-action model with implicit spatial understanding,” *arXiv preprint arXiv:2507.00416*, 2025.

[37] Q. Qian, G. Zhao, G. Zhang, J. Wang, R. Xu, J. Gao, and D. Zhao, “Gp3: A 3d geometry-aware policy with multi-view images for robotic manipulation,” *arXiv preprint arXiv:2509.15733*, 2025.

[38] L. Chen, W. Wang, and P. Mordohai, “Learning the distribution of errors in stereo matching for joint disparity and uncertainty estimation,” in *Proceedings of the IEEE/CVF Conference on Computer Vision and Pattern Recognition*, 2023, pp. 17235–17244.

[39] Z. Shen, Y. Dai, and Z. Rao, “Cfnet: Cascade and fused cost volume for robust stereo matching,” in *Proceedings of the IEEE/CVF conference on computer vision and pattern recognition*, 2021, pp. 13906–13915.

[40] Z. Shen, Y. Dai, X. Song, Z. Rao, D. Zhou, and L. Zhang, “Pcw-net: Pyramid combination and warping cost volume for stereo matching,” in *European conference on computer vision*. Springer, 2022, pp. 280–297.

[41] H. Xu and J. Zhang, “Aanet: Adaptive aggregation network for efficient stereo matching,” in *Proceedings of the IEEE/CVF conference on computer vision and pattern recognition*, 2020, pp. 1959–1968.

[42] B. Liang, Y. Wang, Z. Huang, Z. Hu, H. Hu, J. Xu, and D. Chen, “Arunet: Advancing real-time stereo matching for robotic perception on edge devices,” *IEEE Robotics and Automation Letters*, vol. 10, no. 9, pp. 8970–8977, 2025.

[43] Y. Zhang and J. Zhang, “Gfanet: Group fusion aggregation network for real time stereo matching,” *IEEE Robotics and Automation Letters*, vol. 8, no. 7, pp. 4251–4258, 2023.

[44] L. Lipson, Z. Teed, and J. Deng, “Raft-stereo: Multilevel recurrent field transforms for stereo matching,” in *2021 International Conference on 3D Vision (3DV)*. IEEE, 2021, pp. 218–227.

[45] G. Xu, X. Wang, X. Ding, and X. Yang, “Iterative geometry encoding volume for stereo matching,” in *Proceedings of the IEEE/CVF conference on computer vision and pattern recognition*, 2023, pp. 21919–21928.

[46] J. Li, P. Wang, P. Xiong, T. Cai, Z. Yan, L. Yang, J. Liu, H. Fan, and S. Liu, “Practical stereo matching via cascaded recurrent network with adaptive correlation,” in *Proceedings of the IEEE/CVF conference on computer vision and pattern recognition*, 2022, pp. 16263–16272.

[47] J. Jing, J. Li, P. Xiong, J. Liu, S. Liu, Y. Guo, X. Deng, M. Xu, L. Jiang, and L. Sigal, “Uncertainty guided adaptive warping for robust and efficient stereo matching,” in *Proceedings of the IEEE/CVF International Conference on Computer Vision*, 2023, pp. 3318–3327.

[48] R. Gong, W. Liu, Z. Gu, X. Yang, and J. Cheng, “Learning intra-view and cross-view geometric knowledge for stereo matching,” in *Proceedings of the IEEE/CVF conference on computer vision and pattern recognition*, 2024, pp. 20752–20762.

[49] Y. Xu, S. Chen, X. Yang, Y. Xiang, J. Yu, W. Ding, J. Wang, and Y. Wang, “Efficient and hardware-friendly online adaptation for deep stereo depth estimation on embedded robots,” *IEEE Robotics and Automation Letters*, vol. 10, no. 5, pp. 4308–4315, 2025.

[50] A. Enyedy, A. Aswale, B. Calli, and M. Gennert, “Stereo image-based visual servoing towards feature-based grasping,” in *2024 IEEE International Conference on Robotics and Automation (ICRA)*. IEEE, 2024, pp. 7325–7331.

[51] R. Singh, A. Allshire, A. Handa, N. Ratliff, and K. Van Wyk, “Dextrah-rgb: Visuomotor policies to grasp anything with dexterous hands,” *arXiv preprint arXiv:2412.01791*, 2024.

[52] T. Kollar, M. Laskey, K. Stone, B. Thananjeyan, and M. Tjersland, “Simnet: Enabling robust unknown object manipulation from pure synthetic data via stereo,” in *Conference on Robot Learning*. PMLR, 2022, pp. 938–948.

[53] Z. Cai, M. Cao, H. Chen, K. Chen, K. Chen, X. Chen, X. Chen, Z. Chen, Z. Chen, P. Chu *et al.*, “Internlm2 technical report,” *arXiv preprint arXiv:2403.17297*, 2024.

[54] Y. Lipman, R. T. Chen, H. Ben-Hamu, M. Nickel, and M. Le, “Flow matching for generative modeling,” *arXiv preprint arXiv:2210.02747*, 2022.

[55] M. Oquab, T. Darce, T. Moutakanni, H. Vo, M. Szafraniec, V. Khalidov, P. Fernandez, D. Haziza, F. Massa, A. El-Nouby *et al.*, “Dinov2: Learning robust visual features without supervision,” *arXiv preprint arXiv:2304.07193*, 2023.

[56] A. O’Neill, A. Rehman, A. Maddukuri, A. Gupta, A. Padalkar, A. Lee, A. Pooley, A. Gupta, A. Mandlekar, A. Jain *et al.*, “Open x-embodiment: Robotic learning datasets and rt-x models: Open x-embodiment collaboration 0,” in *2024 IEEE International Conference on Robotics and Automation (ICRA)*. IEEE, 2024, pp. 6892–6903.

[57] E. Todorov, T. Erez, and Y. Tassa, “Mujoco: A physics engine for model-based control,” in *2012 IEEE/RSJ International Conference on Intelligent Robots and Systems*. IEEE, 2012, pp. 5026–5033.

[58] NVIDIA, “Isaac Sim.” [Online]. Available: <https://github.com/isaac-sim/IsaacSim>

[59] Z. Peng, W. Wang, L. Dong, Y. Hao, S. Huang, S. Ma, and F. Wei, “Kosmos-2: Grounding multimodal large language models to the world,” *ArXiv*, vol. abs/2306.14824, 2023.

[60] J. Wang, M. Chen, N. Karaev, A. Vedaldi, C. Rupprecht, and D. Novotny, “Vggt: Visual geometry grounded transformer,” in *Proceedings of the Computer Vision and Pattern Recognition Conference*, 2025, pp. 5294–5306.

[61] D. Eigen, C. Puhrsch, and R. Fergus, “Depth map prediction from a single image using a multi-scale deep network,” in *Advances in neural information processing systems*, 2014.